ELSEVIER

Journal of Volcanology and Geothermal Research 110 (2001) 299–318

Journal of volcanology and geothermal research

www.elsevier.com/locate/jvolgeores

# Late Precambrian Balkan-Carpathian ophiolite — a slice of the Pan-African ocean crust?: geochemical and tectonic insights from the Tcherni Vrah and Deli Jovan massifs, Bulgaria and Serbia

Ivan Savov[a,*], Jeff Ryan[a], Ivan Haydoutov[b], Johan Schijf[c]

[a]*Department of Geology, University of South Florida, 4202 E. Fowler Ave., SCA 520, Tampa, FL 33620-5201, USA*
[b]*Bulgarian Academy of Sciences, Geological Institute, Sofia 1113, Bulgaria*
[c]*Department of Marine Science, University of South Florida, 140 7th Ave S, St. Petersburg, FL 33701, USA*

**Abstract**

The Balkan-Carpathian ophiolite (BCO), which outcrops in Bulgaria, Serbia and Romania, is a Late Precambrian (563 Ma) mafic/ultramafic complex unique in that it has not been strongly deformed or metamorphosed, as have most other basement sequences in Alpine Europe. Samples collected for study from the Tcherni Vrah and Deli Jovan segments of BCO include cumulate dunites, troctolites, wehrlites and plagioclase wehrlites; olivine and amphibole-bearing gabbros; anorthosites; diabases and microgabbros; and basalts representing massive flows, dikes, and pillow lavas, as well as hyaloclastites and umbers (preserved sedimentary cover). Relict Ol, Cpx and Hbl in cumulate peridotites indicate original orthocumulate textures. Plagioclase in troctolites and anorthosites range from $An_{60}$ to $An_{70}$. Cumulate gabbro textures range from ophitic to poikilitic, with an inferred crystallization order of Ol-(Plag + Cpx)-Hbl. The extrusive rocks exhibit poikilitic, ophitic and intersertal textures, with Cpx and/or Plag (Oligoclase-Andesine) phenocrysts. The major opaques are Ti-Magnetite and Ilmenite. The metamorphic paragenesis in the mafic samples is Chl-Trem-Ep, whereas the ultramafic rocks show variable degrees of serpentinization, with lizardite and antigorite as dominant phases. Our samples are compositionally and geochemically similar to modern oceanic crust. Major element, trace element and rare earth element (REE) signatures in BCO basalts are comparable to those of MORB. In terms of basalt and dike composition, the BCO is a 'high-Ti' or 'oceanic' ophiolite, based on the classification scheme of Serri [Earth Planet. Sci. Lett. 52 (1981) 203]. Our petrologic and geochemical results, combined with the tectonic position of the BCO massifs (overlain by and in contact with Late Cambrian island arc and back-arc sequences), suggest that the BCO may have formed in a mid-ocean ridge setting. If the BCO records the existence of a Precambrian ocean basin, then there may be a relationship between the BCO and the Pan-African ophiolites from the Arabian–Nubian Shield. We suggest that the BCO is the missing link between the Pan-African and the Avalonian–Cadomian peripheral orogens of Murphy and Nance [Geology 19 (1995) 469]. 

*Keywords*: MORB; ophiolite; Precambrian; Pan-African-Cadomian connection; Balkan-Carpathian region

## 1. Introduction

The volcanic and intrusive rock associations preserved in ophiolite complexes offer a means of assessing the processes and conditions of basaltic magmatism through time. Ophiolites are also useful in the reconstruction of a region's tectonic history, as these units indicate the presence of sutures and the closure of ancient marine basins. The lithologic associations and the chemical signatures of ophiolitic rock units can provide further tectonic insights, as complexes formed in arc, back-arc, and oceanic

* Corresponding author. Tel.: +1-813-974-6287; fax: +1-813-974-2654.
*E-mail address:* isavovl@luna.cas.usf.edu (I. Savov).

0377-0273/01/$ - see front matter 
PII: S0377-0273(01)00216-5

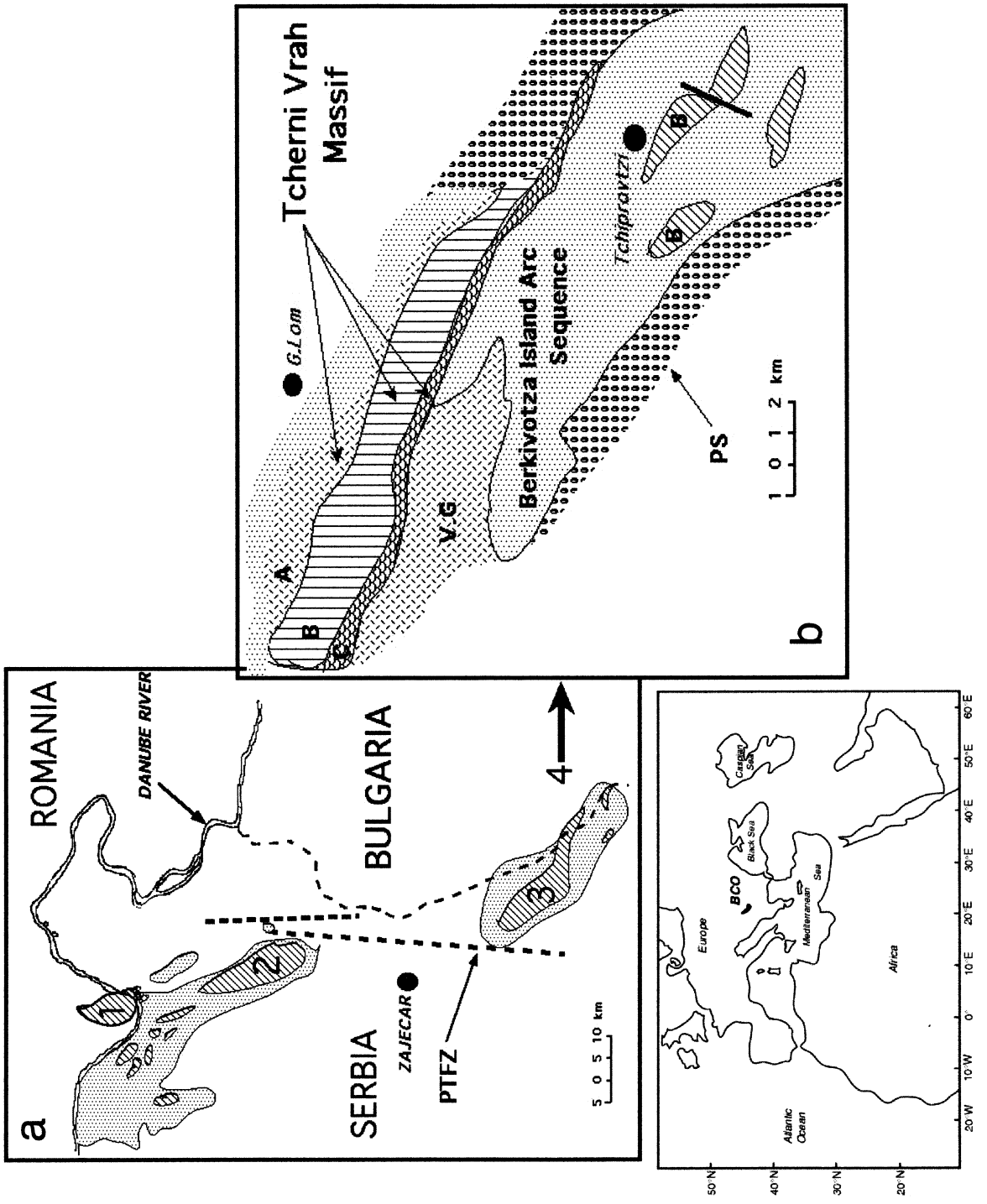
a
ROMANIA
DANUBE RIVER
BULGARIA
SERBIA
ZAJECAR
PTFZ
1
2
3
4
5 0 5 10 km
b
Tcherni Vrah
Massif
6.Lom
A
B
C
V.G
Berkivotza Island Arc
Sequence
Tchiprovtzi
PS
1 0 1 2 km
Europe
Africa
Atlantic
Ocean
Black Sea
Caspian
Sea
Mediterranean
Sea
BCO
20 W
10 W
0
10 E
20 E
30 E
40 E
50 E
60 E
50 N
40 N
30 N
20 N

settings can often be differentiated based upon cumulate sequences and the chemical signatures of their basaltic volcanics (Pearce, 1982; Shervais, 1982; Beccaluva et al., 1979). Precambrian ophiolites are thus especially valuable as indicators of changing igneous processes and ocean development through Earth history. Unfortunately, ongoing tectonic processes at the Earth's surface, and in crust, can disaggregate, deform and metamorphose ancient ophiolitic rocks so extensively that it is often a significant achievement to recognize them as being ophiolitic in character (see Tenthorey et al., 1996; Berger et al., 2001; for discussions of possible ophiolitic rocks in the southern US Appalachians). Thus a well-preserved and relatively unmetamorphosed ophiolite of Precambrian age is a geologic resource of particular value.

Such a well-preserved ancient ophiolite complex exists in the Balkan mountains of Southeastern Europe. Named the Balkan-Carpathian ophiolite (BCO) by Haydoutov (1991), this complex includes several major massifs, which may be fault-block remnants of a single ophiolite thrust sheet (Haydoutov, 1991). Stratigraphic relations and paleontological evidence place these units below earliest Cambrian volcanic and sedimentary sequences (Kalenic, 1986; Kalvacheva, 1986), and newly reported radiometric dates from a BCO gabbro suggest an age greater than 560 Ma (Quadt et al., 1998). Results on a selection of BCO basaltic volcanic rocks indicate very low metamorphic grades (greenschist facies) and compositions suggesting oceanic affinities (Haydoutov, 1991).

The goal of this study is to extend our knowledge of the petrologic relationships among the different mafic/ultramafic assemblages within the BCO, testing the contention of Haydoutov (1991) that the different BCO massifs have similar origins and evolutionary paths. Through petrographic and geochemical examination of a spectrum of BCO volcanic and cumulate rocks, we will characterize the BCO in light of the diversity of ophiolites, and through comparisons to modern oceanic volcanic rocks. Our results allow us to address the question of the tectonic environment in which the BCO originated. In particular, we will consider the BCO in the context of Pan-African collisional events which affected Eastern Europe, the Middle East, and NE Africa in the Latest Precambrian.

## 2. Geologic setting

The BCO is one of the largest ophiolite bodies found in the Balkan Peninsula. It comprises several massifs that were emplaced along the Tracian Suture — part of the so-called South European suture (Haydoutov, 1991) (Fig. 1). Similar ophiolite massifs, such as the Kraubath and Hohgrossen massifs in the Eastern Alps (Ageed et al., 1980) outline the South European suture to the west (Haydoutov, 1989). To the east the Bolu massif in Turkey (Goncouglu, 1997; Ustaömer and Kipman, 1997) and the Pan-African ophiolites of the Arabian–Nubian Shield may reflect a continuation of the South European suture. Together these suture zones may represent the trace of the Pan-African (proto-Tethys) ocean (Haydoutov, 1991).

The BCO is exposed as several distinct massifs: the Tcherni Vrah (Bulgaria), Zaglavac and Deli Jovan (Serbia) and South Banat (Romania) massifs (Haydoutov, 1989) (Fig. 1). The Tcherni Vrah and Zaglavac massifs are similar structurally and stratigraphically, and together with Deli Jovan massif, which is separated by the Poretchko–Timoshki fault zone, they comprise a complete ophiolitic sequence (Haydoutov, 1991). These massifs are unconformably overlain by a Cambrian-age volcano-sedimentary and arc-related sequence, known in Bulgaria as the Berkovitza Group and in Serbia as the Vlasinski complex. Based on the occurrence of Archaeocyathids in carbonates of the Vlasinski complex (Kalenic, 1986), the Tcherni Vrah and Deli Jovan massifs were placed in the Late Precambrian–earliest Cambrian. Recent U–Pb zircon dating results of gabbroic rocks from Tcherni Vrah massif confirm a Latest Precambrian age: 563 ± 5 Ma (Quadt et al., 1998).

Fig. 1. (a) Map showing the location of the four different BCO massifs. 1: South Banat massif; 2: Deli Jovan massif; 3: Zaglavac massif; 4: Tcherni Vrah massif. PTFZ: Poretchko–Timoshki fault zone. (b) Major units of the Tcherni Vrah massif. A: Cumulate Unit. B: Sheeted Dykes. C: Pillow Lavas. V.G.: Variscan granitic intrusions. P.S: Permian sediments. Berkivotza Island Arc units overlie Tcherni Vrah.

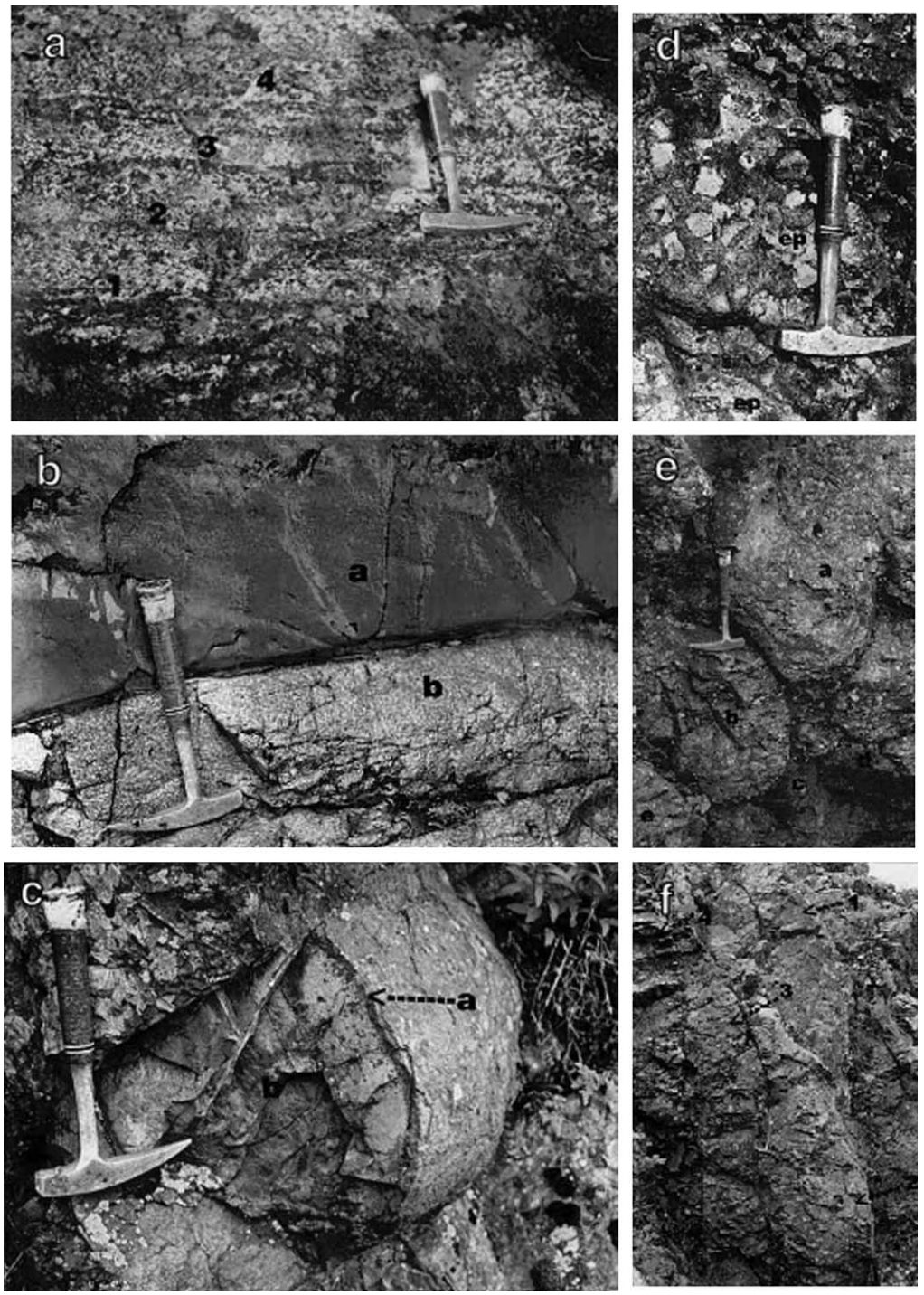


Fig. 2. Field relations in the Tcherni Vrah Massif. (a) Layered gabbros in the Lower Cumulate Unit. (b) Epidote lenses (ep) marking boundary between sheeted dykes and basalts. (c) Sharp boundary between basaltic dyke (a) and evolved microgabbro dyke (b). (d) Chilled margin (a) in pillow lava (b). (e) A system of preserved pillow lavas (a, b, c, d, e). (f) System of preserved lava tubes (1–4) within the Pillow Lavas unit.

For the purposes of our study we have focused on the Tcherni Vrah and Deli Jovan massifs, as they provide excellent exposures and have been well characterized in terms of field relations and major lithologies (Haydoutov, 1989, 1991; Kolcheva and Jordanov, 1984).

## 3. Internal stratigraphy and petrology

*Tcherni Vrah massif:* The Tcherni Vrah massif outcrops in the Stara Planina mountains of NW Bulgaria, and is the best-studied massif within the BCO (Fig. 1B). It includes cumulate, sheeted dyke and pillow lava units (Haydoutov, 1989). In the best-preserved domains of Tcherni Vrah, there are clear similarities between the strike of the sheeted dikes, and in the elongation of preserved lava tubes in the pillow lava unit (see Ballard and Moore, 1977; Haydoutov, 1991). These preserved relationships between different ophiolite units suggest little relative motion has occurred among the units since their formation as igneous sequences (Haydoutov, 1991).

The cumulate section is composed of ultramafic cumulates and gabbros, and has a total thickness of 2.5 km. The unit's lower boundary is tectonic, while the upper boundary grades through isotropic gabbros into sheeted dykes. Mineralogic layering is prominent in outcrop (Fig. 2a). The lower cumulate sequence includes relatively thin (0.15–6 m) alternating layers of gabbros and ultramafic cumulates (wehrlites, plagioclase wehrlites, troctolites, olivine gabbros, pyroxenites and anorthosites). These horizons are distinguished by the gradual appearance of plagioclase. The upper cumulate sequence lacks ultramafic cumulates and is dominated by gabbros. The gabbros alternate with lenses of anorthosite, pyroxenite and pegmatoid gabbro, giving the unit a layered appearance. The thickness of the layers varies from 4 cm in gabbros up to 5–6 m in the wehrlites and troctolites.

The sheeted dykes unit has a total thickness of ~1 km. Its upper boundary is gradational, with dykes crosscutting lava flows of ophitic basalts. Epidote lenses often mark the transition between sheeted dykes and basalts (Fig. 2b). Dykes intrude each other and many exhibit chilled margins (Fig. 2c). Dyke thickness range from 7 to 5 m, and all have similar strikes and dips (~120–140°, and 60–70° to the SW).

The extrusives section at Tcherni Vrah forms a 20-km-long mappable unit with a thickness of 700 m. It consists of alternating pillow lavas, lava tubes and massive basalt flows (Fig. 2 d–f) overlain by hyaloclastites, lava breccias and sediments. Pillow lavas are more abundant than massive flows. Pillow sequences may be up to 150 m thick, while massive flows and hyaloclastites are seldom more than 1–3 m thick. Sediments are preserved as lenses of black phyllites between pillows, or as bedded pink argillites near the top of the unit.

*Deli Jovan massif.* The Deli Jovan massif outcrops in the Deli Jovan mountain of NE Serbia (Fig. 1). It includes ultramafic and mafic cumulates, sheeted dykes and a volcanic section. Based on the relative thicknesses of mafic and ultramafic cumulates at Deli Jovan, Haydoutov (1991) divided the cumulate sequences into eastern and western parts. The eastern part includes layers of dunites, troctolites, olivine gabbros, wehrlites and anorthosites, which alternate with fine-grained gabbros. The western part is composed of coarse-grained (locally pegmatoid), undeformed gabbros with little or no occurrence of ultramafic cumulates. According to Terzic (1981), these gabbros grade stratigraphically upward into a microgabbro/diabasic sheeted dyke unit with a total thickness of ~2 km, and the sheeted dykes grade upwards into unpillowed aphanitic basalts.

## 4. Sampling and analytical methods

Field studies in the summer of 1997 by Savov and Haydoutov confirmed the mapping results and lithologic relationships of Haydoutov (1991). A representative suite of samples from the Tcherni Vrah and Deli Jovan massifs was collected for petrographic and geochemical study. Seventy thin sections were examined for textural and mineralogic relationships. Fifty samples representing all major ophiolite lithologies except pyroxenites were crushed and powdered for chemical analysis. Major and trace element concentrations were determined at the University of South Florida by direct current plasma emission spectrometry (DCP), following $LiBO_2$ fluxed-fusion digestions. Dissolution techniques follow those described by Tenthorey et al. (1996) in that furnace temperatures were maintained at

1115–1125°C to assure complete digestion of ultramafic samples. Precision for major elements varies with element from <1 to 3%. Trace element reproducibility varies strongly with concentration and ranges from ±5 to ±25% (Table 2).

Rare earth element (REE) abundances were measured via ICP-MS, using the FISONS PlasmaQuad PQS instrument at the USF Department of Marine Sciences in St. Petersburg, FL. Samples were dissolved via $Na_2CO_3$ fluxed fusion digestion. In this procedure, a variation on the boron digestion technique of Ryan and Langmuir (1993), 4:1 flux-sample mixtures were heated for ~2 h to 1050°C in Pt crucibles. The fusion cakes were decomposed in DI water at ~100°C, and were then rinsed thoroughly to leach away water-soluble alkalies and $Na_4SiO_4$. The insoluble fraction of the fusion cake, which quantitatively retains the REE, was then dissolved in 1% $HNO_3$ and spiked with 50 ppb each of Re and Cs internal standards. Final dilution factors were 1000:1. No preconcentration or column separation step was included in our procedure.

The PQS instrument utilized a Meinhard nebulizer and a chilled spray chamber for sample injection. Oxide generation was monitored during each run, and was never more than 1–2% (based on CeO determination) during any run. We used a combined calibration procedure, calibrating REE intensities to those of the Re and Cs internal standards, and then generating working curves for the REE using synthetic standard solutions which were matrix matched through the addition of Ca, Mg, and Al to a total concentration of ~400 ppm.

Working detection limits for the REE on the ICP-MS are a strong function of both the in-rock concentrations and the isotopic distributions of the elements being examined. For any particular REE mass, solution detection limits are on the order of 0.01 ppb, but the combination of multiple masses (which results in reduced signal on a particular mass) and low in-rock concentrations can increase the practical detection limits for a given element considerably. As a result, in-rock detection limits for the REE vary considerably, from 0.5 ppm for Tb, Yb, and Eu to 0.01 ppm for La, Pr, Ce, and Tm. In terms of data interpretation, the detection limit for Eu is particularly problematic in that Eu contents in the volcanic and diabasic rocks were measurable, while Eu in many of the cumulate rocks was not.

Table 1
REE data comparisons

| BIR-1, USGS Islandic basalt | | |
|---|---|---|
| Element | Avg[a] (ppm) | Rec. value |
| La | 0.39 | 0.88 |
| Ce | 1.69 | ~2.5[b] |
| Pr | 0.38 | ~0.5[b] |
| Nd | 1.94 | 2.5 |
| Sm | 1.04 | ~1.08[b] |
| Eu | 0.26 | ~0.54[b] |
| Gd | 1.63 | 1.9 |
| Dy | 2.42 | ~2.4[b] |
| Ho | 0.57 | 0.5 |
| Er | 1.69 | 1.8 |
| Tm | 0.26 | 0.27 |
| Lu | 0.25 | 0.26 |

[a] Average of four separate ICP-MS analyses.
[b] USGS suggested value only.

REE reproducibility was on the order of ±10%. Replicates of USGS standard basalts BIR-1, BHVO-1 and W-2 as well as NBS standard 688 are within 10% of the reported values except at the very lowest REE contents (Table 1).

## 5. Results

*Petrography*. All ultramafic cumulate samples show mineral assemblages, which reflect lower greenschist facies metamorphic conditions, but relict olivine and clinopyroxene grains are relatively common. Primary amphibole is present in some cumulate thin sections and may represent near-solidus crystallization in a cooling ophiolite magma chamber (Herbert and Laurent, 1990). The dunites are pervasively serpentinized, and the serpentines exhibit typical mesh and hourglass textures (Fig. 3a). The principal opaque appears to be magnetite, as it is locally altered to hematite. Primary minerals in the wehrlites are olivine, clinopyroxene and amphibole. Olivine grains preserve original crystal shapes and locally form layers, which suggests cumulate origins. The clinopyroxenes are pale green in thin section, and occur as euhedral grains interstitial among the olivines. Secondary amphibole is found rimming

both olivine or clinopyroxene grains. Troctolites from Deli Jovan are generally fresh, while those from Tcherni Vrah are altered. The primary minerals are plagioclase, olivine, and clinopyroxene, with accessory spinel-group minerals (Fig. 3b). Plagioclase is typically ~$An_{70}$ (bytownite) and forms thick prismatic laths exhibiting combined albite and Carlsbad twinning. Rodingite assemblages (tremolite + hydrogarnet + clinozoisite + epidote ± hedenbergite) derived from the alteration of plagioclase occur in the lower cumulates. Olivine is present as rounded grains that are sometimes rimmed by clinopyroxene. Primary clinopyroxene occurs as short prismatic grains, which often show exsolution effects. Red–brown amphibole coronas locally surround clinopyroxenes. The troctolites show both ophitic and poikilitic textures. Anorthosites are relatively uncommon and show adcumulus textures. The plagioclases in the anorthosites are labradorite in composition (~$An_{55}$).

BCO gabbroic rocks range widely in the relative proportions of plagioclase, clinopyroxene, amphibole and olivine (Fig. 3c). Texturally, these rocks are dominantly pyroxene-plagioclase-olivine cumulates. Plagioclase compositions range from bytownite (~$An_{75}$) to andesine (~$An_{50}$), with the more albitic compositions occurring in the upper gabbros. Greenish clinopyroxene crystals occur interstitially among early-formed plagioclases. In gabbros from Deli Jovan, clinopyroxene may poikilitically enclose plagioclase laths. Gabbroic clinopyroxenes are often rimmed by red–brown amphibole. Olivine, where present, preserves its crystal forms but is commonly altered to a fine-grained aggregate of serpentine, tremolite and chlorite. Amphibole derived from clinopyroxene alteration can comprise up to 45% of the

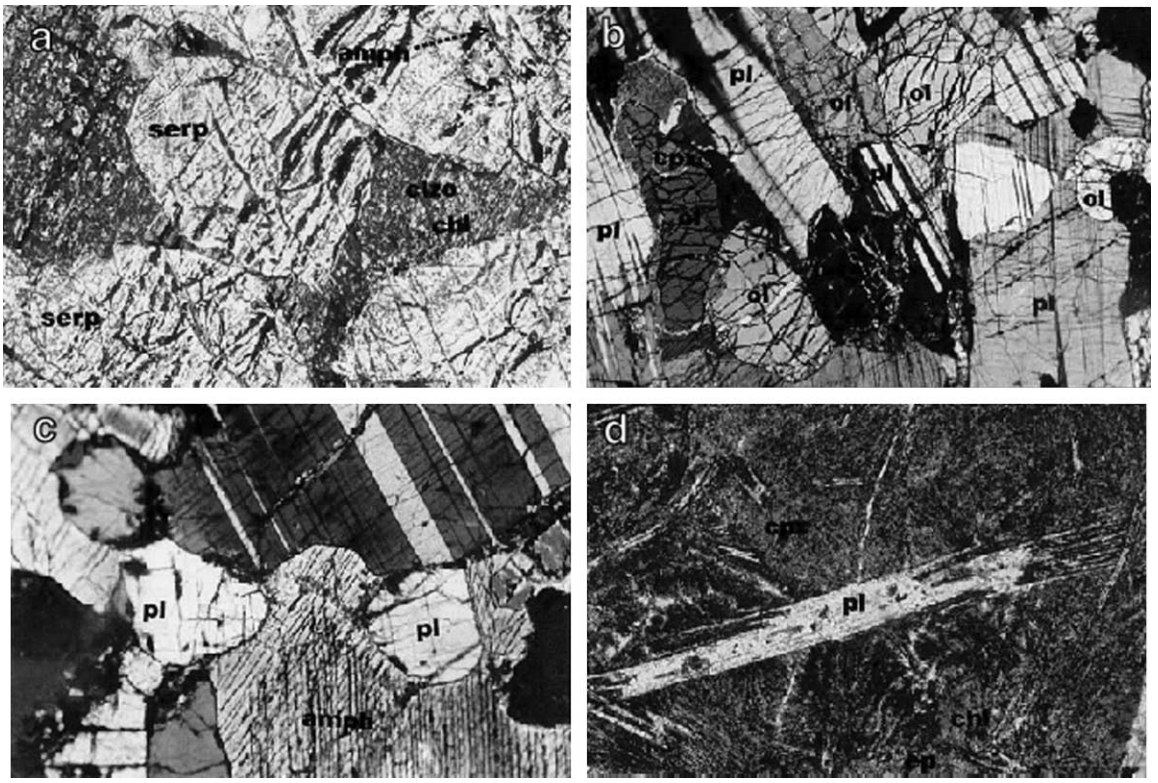


Fig. 3. Photomicrographs of BCO samples. (a) Serpentinized dunite from Deli Jovan with preserved cumulate textures. (b) Fresh troctolite from Deli Jovan with ophitic texture. (c) Amphibole-bearing gabbro from the Upper Cumulate Unit in Tcherni Vrah. (d) Swallow-tail plagioclase phenocryst in variolitic basalt from Tcherni Vrah pillow lavas.

rocks. However, magmatic amphibole,which forms distinct prismatic crystals which are not associated with clinopyroxene, can comprise up to 10% of some rocks (Kolcheva and Jordanov, 1984). Accessory phases include sphene, apatite, ilmenite and magnetite. Alteration assemblages include amphibole + chlorite + epidote.

Diabases consist of plagioclase and augite in varying proportions. Plagioclase forms large, prismatic phenocrysts. Textures are phaneritic and rarely poikilitic. Sometimes pyroxene is rimmed by brown amphibole. Accessory minerals are Ti-magnetite (locally altered to sphene and ilmenite), apatite and zircon. Opaques and accessory minerals may comprise 2–4% of the rock. Plagioclases in more altered horizons of both the dykes and volcanics are often albitized, as can occur during sub-seafloor metamorphism, though in these rocks such an origin is highly speculative.

Basalts range from very fine-grained to aphanitic-porphyritic. Plagioclases form swallow-ended phenocrysts and range compositionally from andesine to nearly pure albite (Fig. 3d). Together with feather-like skeletal clinopyroxene aggregates, these crystals indicate fast cooling rates. Volcanic glass (now an ultra-fine grained matrix) can make up ~85% of the rock. Textures range from ophitic to variolitic and spherolitic in the volcanic glass-rich basalts. Accessory minerals (~2%) are apatite, zircon, sphene, Ti-magnetite and ilmenite.

Based on textural relations in the cumulate and volcanic rocks, the order of crystallization in Tcherni Vrah and Deli Jovan massif samples is olivine ± spinel − plagioclase ≈ clinopyroxene ± amphibole.

## 6. Bulk chemistry

### 6.1. Major and trace elements

Tables 2–6 list our major and trace element results from different units of the BCO. The overall low metamorphic grade of the BCO allows us to study geochemical profiles through the complex, much as

Table 2
Ultramafic cumulates

| Location | Deli Jovan | | | | | Kopilovzi | | | | |
|---|---|---|---|---|---|---|---|---|---|---|
| Rock type | Dunite | Troctolites | | | | Wehrlite | Anorth. | Wehrlite | Troctolite | Gabbroid |
| Sample | DU-5 | TR-1 | TR-2 | TR-3 | TR-4 | SAM1-77 | AN-9/77 | LR-22 | TR-24 | GB-23 |
| Si (wt%) | 42.47 | 47.62 | 44.39 | 45.95 | 44.94 | 41.34 | 44.68 | 40.79 | 42.32 | 47.73 |
| Mn (wt%) | 0.36 | 0.08 | 0.09 | 0.09 | 0.10 | 0.21 | 0.11 | 0.22 | 0.21 | 0.14 |
| Fe (wt%) | 12.49 | 5.65 | 6.40 | 6.03 | 7.27 | 16.93 | 8.08 | 16.56 | 18.90 | 9.81 |
| Ti (wt%) | 0.03 | 0.23 | 0.12 | 0.10 | 0.10 | 0.14 | 0.13 | 0.15 | 0.39 | 0.62 |
| Mg (wt%) | 42.87 | 9.72 | 16.58 | 13.85 | 17.42 | 32.07 | 13.70 | 31.98 | 30.99 | 13.66 |
| Ca (wt%) | 0.00 | 12.62 | 10.01 | 10.62 | 9.75 | 2.85 | 11.23 | 3.32 | 2.72 | 9.34 |
| Al (wt%) | 1.66 | 23.14 | 18.11 | 22.63 | 19.78 | 7.17 | 21.01 | 5.86 | 4.60 | 15.69 |
| K (wt%) | 0.00 | 0.06 | 0.03 | 0.03 | 0.03 | 0.02 | 0.03 | 0.03 | 0.04 | 0.09 |
| Na (wt%) | 0.00 | 1.83 | 1.28 | 1.53 | 1.38 | 0.06 | 1.61 | 0.10 | 0.37 | 2.77 |
| Total | 99.87 | 100.95 | 98.42 | 98.41 | 100.76 | 100.81 | 100.59 | 99.00 | 100.55 | 99.84 |
| LOI (%) | 13.76 | 5.22 | 3.09 | 2.51 | 4.56 | 11.18 | 6.09 | 10.64 | 9.68 | 5.37 |
| Sr (ppm) | 5 | 111 | 112 | 204 | 141 | 24 | 260 | 28 | 31 | 696 |
| Ba (ppm) | 17 | 17 | 11 | 63 | 9 | 8 | 10 | 55 | 25 | 40 |
| Ni (ppm) | 2617 | 267 | 597 | 439 | 1523 | 1351 | 1073 | 1819 | 1958 | 1388 |
| Sc (ppm) | 14 | 34 | 45 | 28 | 14 | 12 | 11 | 13 | 21 | 26 |
| Cr (ppm) | 10041 | 180 | 575 | 251 | 161 | 153 | 234 | 126 | 320 | 344 |
| V (ppm) | 144 | 217 | 169 | 162 | 79 | 52 | 60 | 59 | 79 | 126 |
| Zn (ppm) | 178 | 52 | 54 | 60 | 76 | 84 | 67 | 111 | 113 | 74 |
| Cu (ppm) | 1001 | 40 | 104 | 27 | 63 | 20 | 40 | 23 | 18 | 30 |

Table 3
Gabbroic cumulates

| Rock type | Lower gabbros | | | | Upper gabbros unit | | |
|---|---|---|---|---|---|---|---|
| Location | G.Lom | | | | Sikole | Kitka | |
| Sample | GB-4 | GB 5 | GB-6 | GB-7 | GB-20 | GB-1 | GB-2 |
| Si (wt%) | 50.68 | 48.35 | 49.78 | 53.40 | 49.69 | 49.97 | 50.42 |
| Mn (wt%) | 0.11 | 0.11 | 0.15 | 0.06 | 0.08 | 0.12 | 0.11 |
| Fe (wt%) | 5.62 | 6.96 | 8.15 | 2.60 | 3.92 | 6.81 | 5.58 |
| Ti (wt%) | 0.34 | 0.15 | 0.41 | 0.25 | 0.42 | 0.37 | 0.37 |
| Mg (wt%) | 10.88 | 12.20 | 8.86 | 2.14 | 6.44 | 11.17 | 9.06 |
| Ca (wt%) | 13.90 | 10.77 | 12.39 | 11.94 | 14.95 | 14.13 | 15.10 |
| Al (wt%) | 15.96 | 19.38 | 15.26 | 23.86 | 21.05 | 16.50 | 16.71 |
| K (wt%) | 0.83 | 0.81 | 0.08 | 0.08 | 0.12 | 0.11 | 0.13 |
| Na (wt%) | 1.91 | 1.74 | 2.45 | 4.70 | 2.37 | 1.76 | 1.92 |
| Total | 100.23 | 100.47 | 99.54 | 99.02 | 99.03 | 100.94 | 99.40 |
| LOI (%) | 4.37 | 4.40 | 1.99 | 1.35 | 2.11 | 2.89 | 2.08 |
| Sr (ppm) | 130 | 141 | 141 | 244 | 112 | 138 | 127 |
| Ba (ppm) | 110 | 146 | 16 | 41 | 8 | 10 | 13 |
| Ni (ppm) | 2173 | 1259 | 2368 | 188 | 1350 | 844 | 98 |
| Sc (ppm) | 46 | 23 | 40 | 21 | 18 | 18 | 49 |
| Cr (ppm) | 533 | 323 | 107 | 56 | 525 | 464 | 672 |
| V (ppm) | 175 | 97 | 176 | 121 | 86 | 97 | 211 |
| Zn (ppm) | 56 | 68 | 57 | 54 | 65 | 68 | 58 |
| Cu (ppm) | 86 | 153 | 50 | 26 | 84 | 74 | 100 |

is done in younger ophiolites. We can thus compare the BCO directly with other ophiolites throughout the world (see references in Nicolas, 1989). Data for elements known to be mobilized during low-grade metamorphism (i.e. K, Sr, Ba, Na) are treated with caution (Staudigel and Hart, 1983; Frey et al., 1985; Bodinier et al., 1988; Kepezhinskas et al., 1995). Of our samples, those that show the most pervasive metamorphic alteration are the dunites, wehrlites, lherzolites and troctolites, which have the highest loss on ignition (LOI) values (Table 2). The examined BCO gabbroic and diabasic rocks have moderate to low LOI values (1.3–4.4%) consistent with their relatively pristine character in thin section (Tables 3–5; Fig. 3).

Our BCO samples show a range in bulk composition most closely consistent with mid-ocean cumulate and volcanic rocks. Basalt MgO abundances range from 7.0–9.7 wt%, and do not extend to the lower values encountered in back-arc settings. (Fig. 4a and b) Mean $TiO_2$ contents in the basalts (1.45–1.83 wt%) are comparable to MORBs at similar MgO (Fig. 4a). The sheeted dykes show greater compositional diversity than the basalts (4.35–10.4% MgO; 0.77–2.18% $TiO_2$), but their mean $TiO_2$ and MgO values are similar. Elevated $Na_2O$ contents in some basalts and dykes (2.24–5.17 wt%) suggest alteration, possibly related to exchanges with seawater. Variations in Ca and in Al abundances in BCO cumulate rocks (Tables 2 and 3; Fig. 4b) may suggest an important role for plagioclase crystallization/accumulation in the BCO magma chamber. In Fig. 5a, a plot of FeO/FeO + MgO vs. $TiO_2$ (Serri, 1981), almost all BCO basaltic rocks fall in the high-Ti ophiolite field. On a range of discrimination diagrams (Fig. 5b–d) rocks from the extrusive section of BCO appear indistinguishable from modern ocean ridge basalts. Our samples lack the high Al, low $FeO^*$ (total Fe) and low $TiO_2$ considered by some authors to be the signature of back-arc basalts (patterns which reflect higher $H_2O$ contents in backarc magmas) (Fryer, 1995; Hawkins, 1995; Stolper and Newman 1994). Both the basalts and diabases have relatively high Cr (281 ppm) and Ni (203 ppm) contents, typical of

Table 4
Sheeted dykes unit

| Location | G.Lom | | | | | Ostra Tchuka | | G.Lom | | Gnili Dol | Ostra Tchuka | G.Lom | | |
|---|---|---|---|---|---|---|---|---|---|---|---|---|---|---|
| Rock type | Basalt | Basalt | Basalt | Basalt | Basalt | Basalt | Basalt | Diabase | Diabase | Diabase | Microgabbro | Microgabbro | | |
| Sample | BA-16 | BA-12 | BA-11 | BA-10 | BA-9 | DB-4 | DB-5 | DB-17 | DB-15 | GB-24 | BA-5 | GB-18 | GB-19 | GB-14 |
| Si (wt%) | 49.35 | 52.11 | 50.76 | 56.63 | 49.27 | 50.16 | 50.52 | 49.2 | 51.88 | 50.28 | 52.45 | 48.74 | 50.13 | 48.43 |
| Mn (wt%) | 0.14 | 0.11 | 0.17 | 0.14 | 0.19 | 0.21 | 0.21 | 0.16 | 0.09 | 0.15 | 0.12 | 0.12 | 0.13 | 0.1 |
| Fe (wt%) | 11.39 | 10.82 | 12.07 | 11.57 | 12.14 | 11.77 | 11.88 | 10.52 | 11.67 | 9.27 | 8.22 | 8.76 | 8.15 | 7.1 |
| Ti (wt%) | 1.44 | 1.19 | 1.64 | 1.39 | 1.25 | 1.73 | 1.75 | 1.51 | 2.18 | 1.08 | 1.36 | 0.9 | 0.86 | 0.77 |
| Mg (wt%) | 9.18 | 7.66 | 8.80 | 9.71 | 10.38 | 7.22 | 7.27 | 8.24 | 4.39 | 9.23 | 6.93 | 8.3 | 8.28 | 7.31 |
| Ca (wt%) | 9.34 | 6.11 | 6.92 | 1.22 | 3.12 | 11.29 | 11.35 | 10.87 | 8.09 | 12.34 | 8.67 | 13.03 | 12.56 | 11.49 |
| Al (wt%) | 16.50 | 18.09 | 15.49 | 14.46 | 19.12 | 15.19 | 15.26 | 14.43 | 14.37 | 16.16 | 16.75 | 19.82 | 16.77 | 22.28 |
| K (wt%) | 0.10 | 0.16 | 0.06 | 0.31 | 0.29 | 0.10 | 0.09 | 0.05 | 0.07 | 0.07 | 1.28 | 0.18 | 0.17 | 0.38 |
| Na (wt%) | 3.54 | 4.67 | 3.97 | 2.44 | 5.17 | 2.54 | 2.57 | 2.36 | 4.39 | 2.24 | 3.76 | 2.59 | 2.57 | 3.06 |
| P(wt%) | 0.22 | 0.21 | 0.24 | 0.22 | 0.20 | 0.24 | 0.24 | 0.25 | 0.44 | 0.22 | 0.25 | 0.19 | 0.19 | 0.17 |
| Total | 100.96 | 100.92 | 99.88 | 97.86 | 100.94 | 100.19 | 100.91 | 97.34 | 97.11 | 100.83 | 98.51 | 102.46 | 99.63 | 100.92 |
| LOI (%) | 3.37 | 3.87 | 8.36 | 5.62 | 6.20 | 3.55 | 2.56 | 2.73 | 2.21 | 3.3 | 3.41 | 3.36 | 2.42 | 4.14 |
| Sr (ppm) | 178 | 156 | 86 | 17 | 45 | 168 | 141 | 108 | 560 | 145 | 91 | 146 | 177 | 241 |
| Ba (ppm) | 15 | 27 | 15 | 33 | 24 | 15 | 15 | 6 | 46 | 16 | 79 | 12 | 47 | 32 |
| Ni (ppm) | 69 | 72 | 132 | 38 | 91 | 92 | 107 | 1209 | 471 | 340 | 75 | 219 | 132 | 599 |
| Sc (ppm) | 30 | 26 | 38 | 19 | 25 | 41 | 40 | 13 | 249 | 36 | 34 | 34 | 40 | 37 |
| Cr (ppm) | 192 | 142 | 229 | 138 | 244 | 202 | 198 | 646 | 79 | 1032 | 299 | 59 | 318 | 314 |
| V (ppm) | 258 | 212 | 273 | 156 | 200 | 314 | 323 | 84 | 45 | 150 | 198 | 253 | 263 | 213 |
| Zn (ppm) | 36 | 40 | 80 | 71 | 84 | 67 | 62 | 61 | 57 | 56 | 66 | 49 | 54 | 71 |
| Cu (ppm) | 19 | 17 | 135 | 177 | 147 | 39 | 37 | 48 | 21 | 91 | 85 | 29 | 26 | 37 |
| Zr (ppm) | 44 | 43 | 43 | 38 | 37 | 133 | 67 | 52 | 64 | 88 | 110 | 40 | 37 | 34 |
| Y (ppm) | 38 | 41 | 39 | 35 | 28 | 24 | 36 | 42 | 72 | 26 | 29 | 29 | 31 | 26 |

Table 5
Pillow basalts unit

| Rock type | Pillow basalts | | | | | | |
|---|---|---|---|---|---|---|---|
| Location | Gnili Dol | | | | | | |
| Sample | BA-3 | BA-24 | BA-25 | BA-21 | BA-22 | BA-23 | BA-26 |
| Si (wt%) | 49.40 | 54.32 | 51.39 | 47.74 | 48.02 | 50.33 | 49.57 |
| Mn (wt%) | 0.17 | 0.14 | 0.18 | 0.17 | 0.17 | 0.21 | 0.17 |
| Fe (wt%) | 10.43 | 9.58 | 10.73 | 13.01 | 12.00 | 11.17 | 11.18 |
| Ti (wt%) | 1.46 | 1.54 | 1.83 | 1.66 | 1.65 | 1.61 | 1.45 |
| Mg (wt%) | 7.63 | 7.30 | 7.03 | 9.24 | 7.15 | 9.66 | 7.15 |
| Ca (wt%) | 11.65 | 7.20 | 9.12 | 7.71 | 12.42 | 9.22 | 9.40 |
| Al (wt%) | 15.21 | 13.27 | 14.64 | 17.08 | 16.25 | 13.49 | 18.20 |
| K (wt%) | 0.12 | 0.07 | 0.05 | 0.30 | 0.07 | 0.06 | 0.13 |
| Na (wt%) | 2.97 | 4.99 | 3.45 | 3.21 | 2.76 | 3.59 | 3.67 |
| P (wt%) | 0.26 | 0.23 | 0.28 | 0.29 | 0.25 | 0.26 | 0.23 |
| Total | 99.03 | 99.85 | 100.82 | 100.13 | 100.50 | 99.34 | 100.93 |
| LOI (%) | 2.86 | 4.15 | 4.10 | 4.68 | 3.35 | 3.49 | 4.50 |
| Sr (ppm) | 151 | 178 | 117 | 134 | 178 | 57 | 212 |
| Ba (ppm) | 18 | 14 | 25 | 30 | 19 | 16 | 52 |
| Ni (ppm) | 109 | 72 | 63 | 73 | 88 | 120 | 89 |
| Sc (ppm) | 41 | 41 | 38 | 33 | 43 | 42 | 38 |
| Cr (ppm) | 325 | 272 | 197 | 208 | 273 | 272 | 269 |
| V (ppm) | 267 | 287 | 288 | 233 | 299 | 265 | 277 |
| Zn (ppm) | 82 | 66 | 84 | 68 | 90 | 90 | 83 |
| Cu (ppm) | 94 | 26 | 62 | 36 | 72 | 65 | 75 |
| Zr (ppm) | 148 | 68 | 168 | 96 | 58 | 86 | 52 |
| Y (ppm) | 29 | 24 | 30 | 33 | 29 | 29 | 26 |

Table 6
REE data from BCO Basalts and Mafic cumulates

| Sample | La (ppm) | Ce | Pr | Nd | Sm | Eu | Gd | Dy | Ho | Er | Tm | Yb | Lu |
|---|---|---|---|---|---|---|---|---|---|---|---|---|---|
| BA-26 | 3.26 | 9.83 | 1.77 | 9.07 | 3.26 | 1.08 | 4.67 | 5.35 | 1.17 | 3.4 | 0.52 | 2.95 | 0.46 |
| BA-3 | 4.2 | 11.8 | 2.12 | 10.0 | 3.44 | 0.96 | 4.24 | 5.27 | 1.19 | 3.5 | 0.52 | 3.12 | 0.5 |
| BA-22 | 3.63 | 11.7 | 2.11 | 10.6 | 3.78 | 1.03 | 5.06 | 6.04 | 1.29 | 3.79 | 0.55 | 3.34 | 0.52 |
| BA-23 | 3.47 | 10.9 | 1.98 | 10.0 | 3.59 | 0.65 | 4.73 | 5.83 | 1.27 | 3.7 | 0.55 | 3.25 | 0.52 |
| BA-24 | 2.81 | 9.59 | 1.75 | 8.83 | 3.17 | 0.64 | 4.36 | 5.24 | 1.12 | 3.32 | 0.49 | 2.98 | 0.47 |
| BA-25 | 5.34 | 14.7 | 2.59 | 12.8 | 4.35 | 1.17 | 5.61 | 6.75 | 1.48 | 4.24 | 0.63 | 3.76 | 0.6 |
| BA-12 | 9.58 | 21.6 | 3.26 | 13.3 | 3.78 | 0.81 | 4.53 | 5.4 | 1.2 | 3.51 | 0.54 | 3.37 | 0.55 |
| DB-5 | 3.77 | 11.3 | 2.06 | 9.73 | 3.35 | 0.94 | 4.15 | 5.19 | 1.17 | 3.42 | 0.51 | 3.21 | 0.52 |
| GB-19 | 1.88 | 5.93 | 1.11 | 5.58 | 2.13 | 0.72 | 2.76 | 3.5 | 0.76 | 2.19 | 0.32 | 1.8 | 0.3 |
| GB-18 | 2.07 | 5.94 | 1.05 | 4.92 | 1.81 | 0.52 | 2.36 | 3 | 0.66 | 1.91 | 0.28 | 1.57 | 0.26 |
| GB-14 | 1.09 | 3.74 | 0.71 | 3.02 | 1.13 | BDL | 1.33 | 1.82 | 0.4 | 1.2 | 0.18 | 1.05 | 0.18 |
| GB-24 | 2.14 | 6.46 | 1.19 | 5.63 | 2.11 | 0.56 | 2.61 | 3.42 | 0.77 | 2.23 | 0.33 | 1.95 | 0.31 |
| GB-6 | 0.22 | 1.28 | 0.32 | 1.57 | 0.89 | BDL | 1.25 | 1.83 | 0.41 | 1.16 | 0.17 | 0.88 | 0.15 |
| LR-22 | 0.28 | 0.99 | 0.20 | 0.55 | 0.29 | BDL | 0.42 | 0.36 | 0.08 | 0.25 | 0.04 | BDL | 0.04 |
| TR-1 | 0.38 | 1.37 | 0.27 | 1.01 | 0.44 | BDL | 0.55 | 0.64 | 0.14 | 0.42 | 0.06 | BDL | 0.05 |
| GB-23 | 4.06 | 10.2 | 1.55 | 7.16 | 2.23 | 0.61 | 2.85 | 2.78 | 0.57 | BDL | 0.23 | 1.16 | 0.19 |
| GB-2 | 0.19 | 1.26 | 0.31 | 1.56 | 0.86 | BDL | 1.26 | 1.67 | 0.36 | 1.04 | 0.15 | 0.75 | 0.13 |
| GB-20 | 0.34 | 1.60 | 0.35 | 1.76 | 0.90 | BDL | 1.34 | 1.71 | 0.38 | 1.08 | 0.16 | 0.77 | 0.14 |
| GB-24 | 2.19 | 6.83 | 1.23 | 6.08 | 2.24 | 0.63 | 3.08 | 3.68 | 0.79 | 2.31 | 0.33 | 1.94 | 0.31 |
| GB-4 | BDL | 0.82 | 0.23 | 1.18 | 0.75 | BDL | 1.53 | 1.52 | 0.34 | 0.96 | 0.14 | 0.64 | 0.12 |

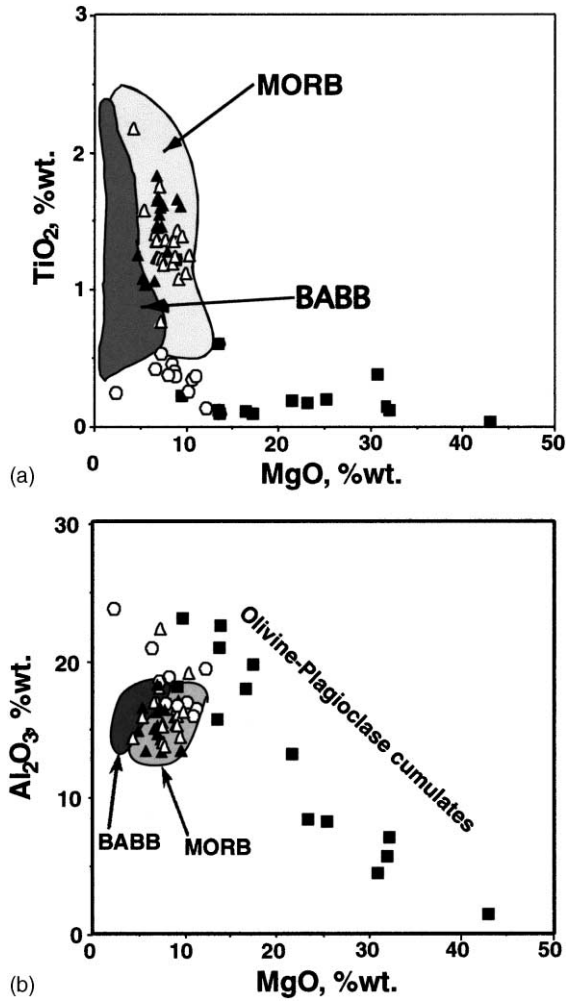


Fig. 4. Major element covariation diagrams for BCO samples. Symbols represent different stratigraphic levels in the ophiolite. Symbols as follows: black squares: ultramafic cumulates; open circles: cumulate gabbros; black triangles: microgabbros and diabase dykes; open triangles: pillowed and massive basalts. (a) $TiO_2$ vs. MgO. MORB field based on data from Ryan (1989) and BVSP (1981) and Klein (pers. comm.). (b) $Al_2O_3$ vs. MgO.

mid-ocean ridge basalts, but not of arc or backarc basalts (Fig. 5b). As well, Shervais (1982) postulates that on a Ti/V discrimination diagram, basalts with backarc origins should plot between the MORB field (Ti/V ratio = 20–50) and island arc field (Ti/V ratio = 10–20). In Fig. 5c, our samples plot entirely in the MORB field, showing little indication of either an arc or backarc origin (Hawkins, 1995; Fryer, 1995).

### 6.2. REE systematics

Twenty-two samples from Tcherni Vrah and Deli Jovan, representing both the upper cumulate and extrusive sections of BCO, were analyzed for REEs (Table 6; Fig. 6). REE patterns for extrusive rocks show low $[La/Sm]_N$ (avg.: 0.63) and $[La/Yb]_N$ (avg.: 0.76) indicative of light rare earth element (LREE) depletion (Fig. 6a and b). BCO cumulates in general show stronger LREE depletions than the basalts, while a few of the more evolved dyke and upper gabbro samples show modestly elevated La/Yb ratios, consistent with extensive fractional crystallization. The segregation of plagioclase crystals is indicated by negative Eu anomalies in the sheeted dykes and basalts (unfortunately, Eu contents in many of our cumulate rocks were below the detection limits of our ICP-MS method). Amphibole accumulation may be indicated by the concave upward shape of REE patterns for some samples from the upper cumulate unit (Fig. 6c). REE abundance patterns thus appear to confirm our petrographic inferences as to the order of crystallization and the crystallizing phases in the BCO rocks. That the REE patterns of the cumulate and extrusive rocks essentially all show strong LREE depletion indicates they were derived from a strongly LREE depleted mantle source, much like modern MORB source regions.

## 7. Discussion

### 7.1. Petrogenesis of the BCO

Our geochemical, petrographic and field results, in concert with earlier work by Haydoutov (1991) allow us to place constraints on the petrogenesis of the BCO complex. Our data support the contention that the two BCO massifs studied represent related cumulate and volcanic igneous rock sequences formed at a mid-ocean ridge. Samples from Deli Jovan and Tcherni Vrah define a single compositional array on the majority of chemical variation diagrams (see Figs. 4–6), which suggests that these massifs represent fragments of a single ophiolitic thrust sheet. The observed transition from the sheeted dykes unit into pillow basalts, and the petrographic and chemical relationships between these units and the cumulates,

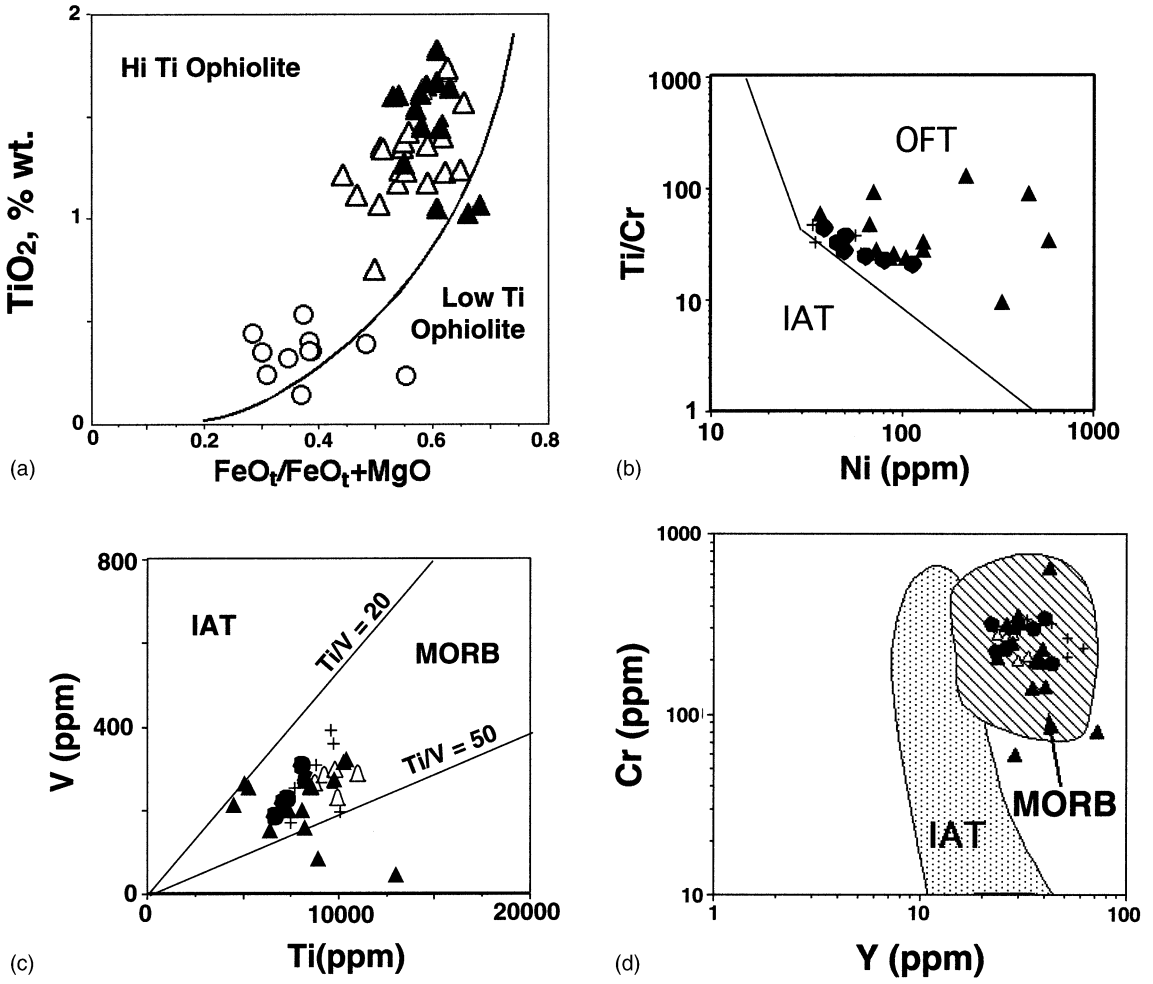


Fig. 5. Trace element based ophiolite discrimination diagrams. Symbols as in Fig. 4. (a) $TiO_2$ vs. Fe/Fe + Mg discrimination diagram after Serri (1981). (b) Ni vs. Ti/Cr discrimination diagram after Beccaluva et al. (1979). IAT: Island Arc Tholeiites; OFT: Ocean Floor Tholeiites. (c) Ti vs. V discrimination diagram after Shervais (1982). IAT: island arc tholeiites. (d) Y vs. Cr discrimination diagram, after Pearce et al. (1982).

are consistent with observations from ODP drilling in modern ocean-ridge settings and with other well-studied, ridge-related ophiolites (Nicolas, 1989).

In terms of both lithophile trace elements and the REE, the extrusive section of the BCO possesses a strongly MORB-like signature (Figs. 5 and 6). All of the basalts are tholeiitic, and the section is thick, which is typical of mature ocean ridge volcanic systems (BVSP, 1981). No cogenetic diorite or trondjhemite intrusions have been discovered, as would be expected in back-arc or arc-related complexes (Nicolas, 1989; Scott et al., 1991; Hawkins, 1995). Also, the sedimentary cover on BCO pillow lavas consists of Fe-rich umbers (with $Fe_2O_3$ contents up to 12.5 wt% (Savov, 1999), typical of deep marine environments, such as can form close to a mid-ocean ridge-crest (Nicolas, 1989). These and other points, (i.e. the inferred order of crystallization in B-C cumulates, the absence of cumulate orthopyroxene (Kolcheva and Jordanov, 1984), geochemical similarities between BCO basalts and MORBs (Fig. 4a; Fig. 5a–d), and compositional similarities between BCO basalts and East Pacific Rise MORB (Melson et al., 1976; Basaltic Volcanism

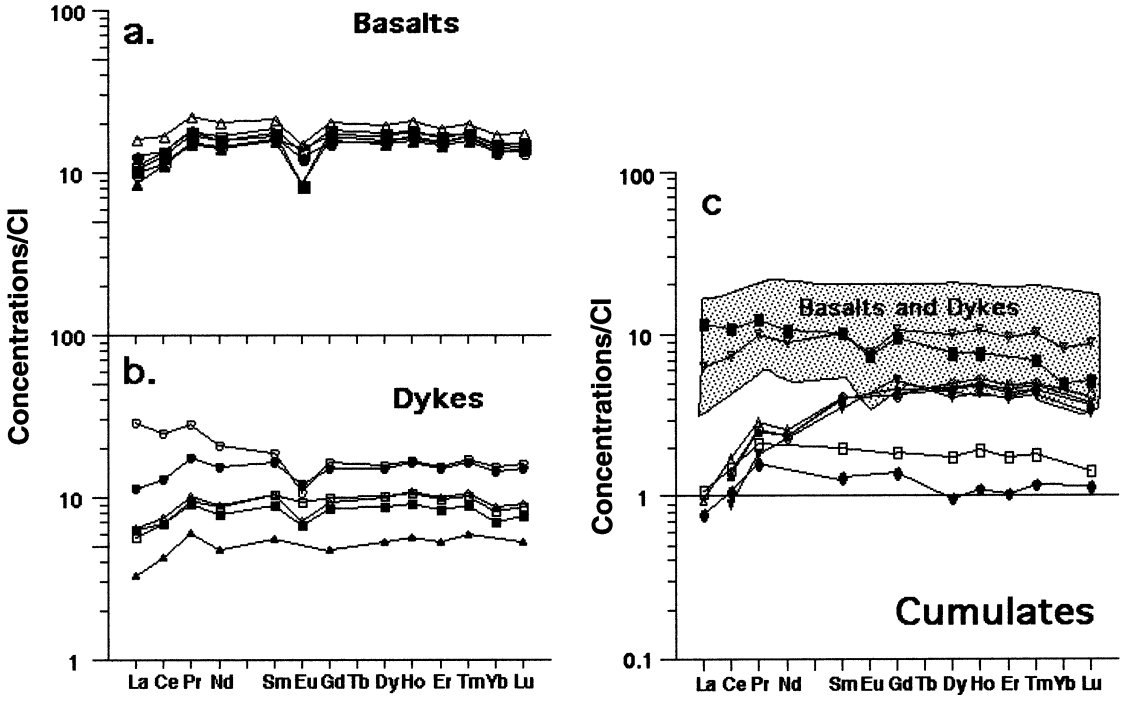


Fig. 6. REE diagrams for the BCO rocks. CI chondritic values from Nakamura (1974). (a) B-C basalts. (b) B-C diabases and microgabbros. (c) B-C cumulate rocks. Shaded fields represent range of B-C basalts and diabases.

Study Project, 1981; Langmuir et al., 1986; Savov, 1999) all suggest a mid-ocean origin for the BCO. Fields for BCO volcanic rocks and for data sets for recent backarc basin basalts (Mariana backarc basin — Stolper and Newman, 1994; Fryer, 1995; Lau backarc basin — Hawkins, 1995; Sumisu Rifts — Hochstaedter et al., 1990); are distinct on all the discrimination diagrams we have examined. Thus, we feel confident in ruling out the possibility of a backarc (suprasubduction zone) origin for the BCO.

### 7.2. Geodynamic implications of the BCO

The petrology and geochemistry of the BCO strongly suggest a mid-ocean origin, which indicates the existence of an oceanic spreading system in the Balkans region during the Latest Precambrian. Together with the overlying Cambrian island-arc sequence, the BCO forms what is known as the Balkan Assemblage (Haydoutov and Yanev, 1997). The Balkan Assemblage is overlain unconformably by an Early Ordovician in age (Kalvacheva, 1986) olistostromal sequence, the Dalgi–Dial Group (Haydoutov, 1991) which contains olistoliths of ophiolitic rocks and igneous rocks of island arc affinities.

Because of its excellent exposure (50,000 $km^2$ of outcrop area) and preservation (only slightly affected by Variscan and Alpine metamorphic events), the Balkan Assemblage can offer insights into the Late Proterozoic–Early Paleozoic tectonic evolution of northwestern Gondwanaland. The BCO is located between the Pan-African ophiolites and the Avalonian–Cadomian peripheral orogens (including the Bohemian massif) and might be the missing link between them (Murphy and Nance, 1995) (Fig. 7). Based both on radiometric and biostratigraphic constraints, the ages of rocks from the Balkan Assemblage straddle the Precambrian–Cambrian boundary (540 Ma; Odin et al., 1983; Compston et al., 1992; Bowring et al., 1993; Bowring and Erwine, 1998), and the age of the BCO (563 ± 5 Ma; Quadt et al., 1998) is Neoproterozoic. The main tectonothermal events of the late Proterozoic (Pan-African) cycle in

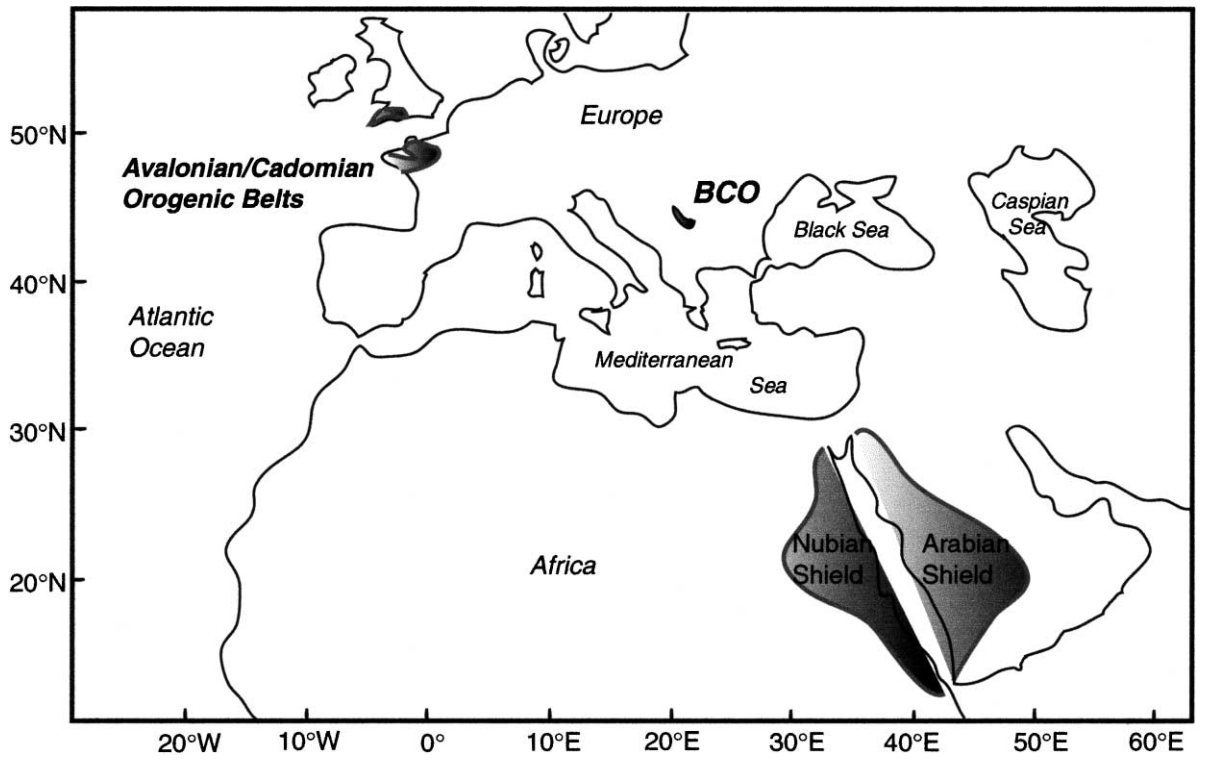


Fig. 7. Regional map of Europe and northern Africa showing the relative positions of the BCO, the rocks of the Arabian–Nubian Shield, and the Avalonian–Cadomian orogenic belts.

Western Gondwana fall in the time range of 650–500 Ma (Kröner, 1984; Unrug, 1993). Thus, the rocks of the Balkan Assemblage are time-correlative with the latter part of the Pan-African orogenic episode (Kröner, 1984).

The Balkan Assemblage, which lies on the margin of the Balkan terrane (Haydoutov and Yanev, 1997), is also proximal to the Arabian–Nubian Shield and the Avalonian–Cadomian peripheral orogens (Murphy and Nance, 1995) (Fig. 7). Comparisons of BCO with ophiolites from the Arabian–Nubian Shield (Abdelsalam and Stern, 1993; Sultan et al., 1993 (for ophiolites from the Nakasib suture); Bakor et al., 1976; Stern et al., 1990 (for ophiolites from the Onib-S. Hamed suture); reveal a number of common features: (e.g. composition of the cumulates (dunites, wehrlites, pyroxenites and gabbros); geochemical affinities of the volcanic rocks to MORB; low metamorphic grade (greenschist facies) (Table 7). The clearest differences between them concern their age, associated sediments and the time span between their age of formation and the time of obduction. Arc-related basement sequences of the Arabian–Nubian Shield show a tendency to become younger from SE to NW, with ages ranging from 900–800 Ma along the southernmost margins of the shield to as young as 540 Ma in the north (Stoeser and Camp, 1985; Stern and Hedge, 1985; Pallister et al., 1988; Almond et al., 1989). The arc-related sequences in the Balkan Assemblage thus appear to be time-correlative with arc-sequences around the NW part of the Arabian–Nubian Shield, another suggestion that BCO and associated rocks may be connected to Pan-African orogenic events (Table 7).

Successor basins developed atop Pan-African age basement rocks appear to have begun receiving sediments between the latest Proterozoic and the early Paleozoic, some as late as the Ordovician, (e.g. Parana Basin; Rogers et al., 1995). In the Murzuk and Wajid basins, the earliest sediments are Cambrian

Table 7
BCO-Pan-African ophiolite comparisons

| Name of complex | Tectonites | Cumulates | Sh. dykes | Geochem. affin. | Met. facies | Associated sediments | Mode of accretion |
|---|---|---|---|---|---|---|---|
| Sol. Hamed (Onib-S. Hamed suture) | Harzburgite | Dunites<br>Wehrlites<br>Pyroxenites<br>Gabbro | 50% | MORB<br>IAT<br>CA | Greenschist | Immature<br>Volcanoclastics<br>Limestones<br>Pelagics | Arc–arc collision emplaced onto volcanogenic sequence |
| Jabal al Wask (Onib-S. Hamed suture) | Harzburgite<br>Dunite | Layered hbl gabbro<br>Two-pyroxene gabbro | – | MORB | Greenschist | Impure limestones<br>Greywackes<br>Distal turbidites | Arc–Arc collision |
| Ophiolite complexes of Nakasib suture | ???????? | Isotropic gabbro<br>Pyroxenite<br>Layered gabbro | – | MORB | Greenschist | Conglomerate and sandstones Lithic wacke and felsic tuff | Emplaced onto passive continental margin |
| BCO (Trachian suture) | Harzburgite<br>Dunite | Isotropic gabbro<br>Wehrlites<br>Pyroxenites<br>Troctolites<br>Layered gabbro | 20% | MORB | Greenschist | Intercalated limestone<br>Umbers (pink phillites) | Emplaced onto passive continental margin |

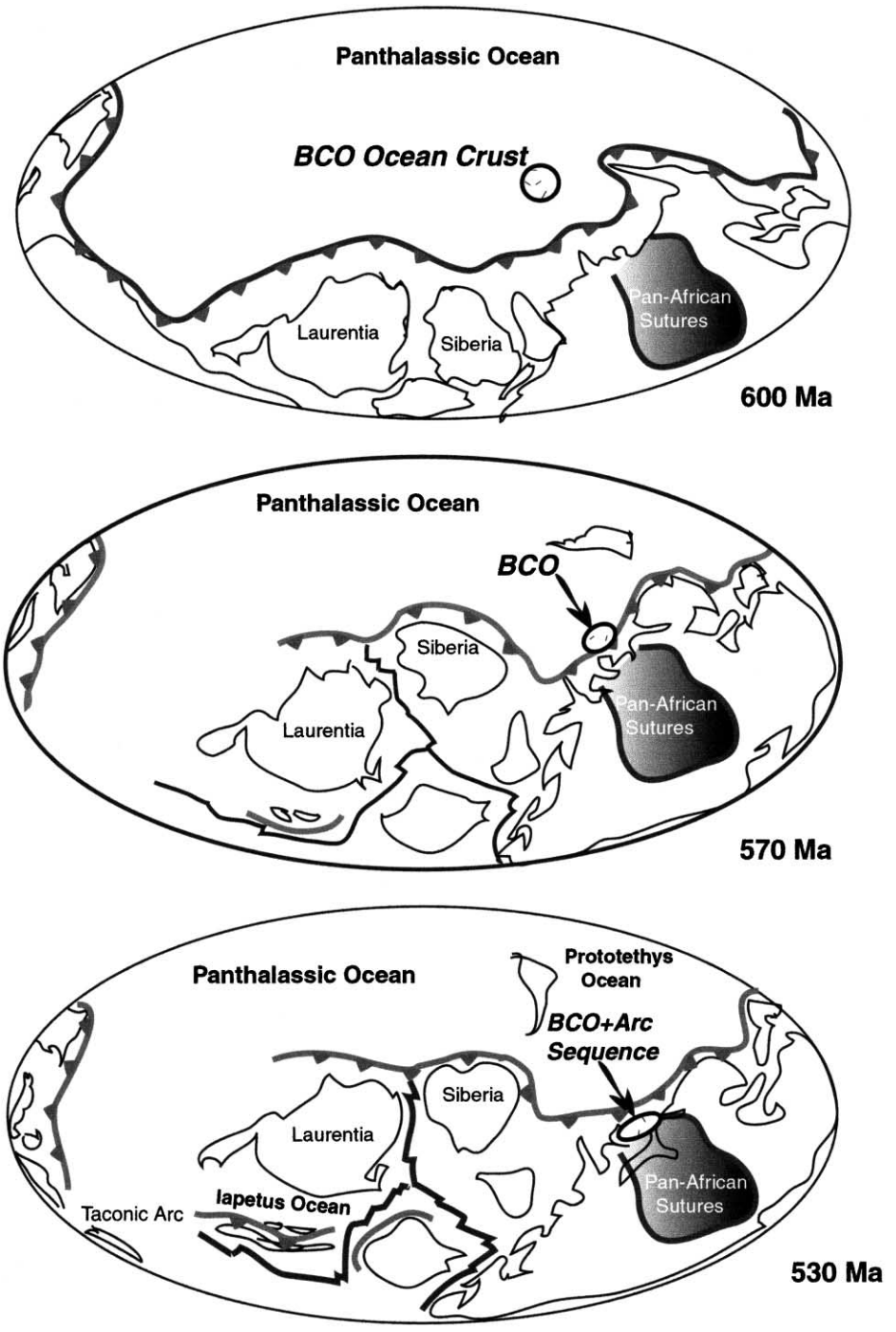


Fig. 8. Paleogeographic maps (modified from Scotese, 1997) showing possible tectonic history of the BCO and associated rocks. Field and geochemical data for BCO indicate an origin as oceanic crust, followed by emplacement in the Cambrian/ Ordovician. (A) 600 Ma. (B) 570 Ma. (C) 530 Ma.

to Ordovician in age (Dabbah and Rogers, 1983). The age of the Dalgi Dial olistostromal sequence, which represents the beginnings of sedimentation in Paleozoic successor basins developed atop Balkan Assemblage rocks is early Ordovician (Kalvacheva, 1986), again consistent with the age distributions for orogenic and post-orogenic events in the Pan-African orogeny. Thus, both geochemically and tectonically, the BCO is consistent with an origin in the Proto-Tethys ocean and emplacement during the later stages of the Pan-African collisional event (Fig. 8).

## 8. Conclusions

The Deli Jovan and Tcherni Vrah ophiolitic massifs are fragments of a single Balkan-Carpathian ophiolitic massif. The BCO overall shows mid-ocean ridge affinities, and may represent a crustal fragment from a large oceanic basin. The BCO and overlying arc-related sequences of the Balkan Assemblage, along with the olistrostromal sequences of the overlying Dalgi–Dial group, show strong chronologic connections to events in the later portions of the Pan-African orogeny, as recorded in units along the margins of the Arabian–Nubian Shield. We thus suggest that the BCO represents crustal rocks from the Proto-Tethys ocean basin emplaced in the closing stages of the Pan-African collision.

## Acknowledgements

Many thanks to all the people who made this project possible: Kristina Kolcheva for her thoughtful review on our petrography and for her contribution to the sample set. Reviews by Kevin Hefferan, Pavel Kepezhinskas, Bill Muerer, Jean Bedard and Yakim Dilek significantly improved this paper. Chris Scotese and Ronald Blakey provided help with the paleo-geographic maps. Emily Klein allowed the use of the GERM Project MORB data. Most of this study was funded, thanks to grants from the Sigma Xi to Ivan Savov and USF Department of Geology.

## References

Abdelsalam, M.G., Stern, R.J., 1993. Structure of the late Proterozoic Nakasib suture, Sudan. J. Geol. Soc. London 150, 393–404 (see also pages 1065–1074).

Ageed, A., Saager, R., Stumfl, E., 1980. Pre-alpine ultramafic rocks in the Eastern Central Alps, Austria. In: Ophiolites: Cyprus, Panayotou, A. (Ed.). Proc. Int. Ophiolite Symp., 601–606.

Almond, D.C., Dabyshire, D.P.F., Ahmed, F., 1989. Age limit for major shearing epizodes in the Nubian Shield of NE Sudan. J. Afr. Earth Sci. 9, 489–496.

Bakor, A.R., Gass, I.G., Neary, C.R., 1976. Jabal al Wask, Northwest Saudi Arabia: an Eocambrian back-arc ophiolite. Earth Planet. Sci. Lett. 30, 1–9.

Ballard, R., Moore, J., 1977. Photographic Atlas of the Mid-Atlantic Ridge Rift Valley. Springer, New York, p. 114.

Beccaluva, L., Ohnenstetter, D., Ohnenstetter, M., 1979. Geochemical discrimination between ocean floor and island arc tholeiites — Application to some ophiolites. Can. J. Earth Sci. 16, 1874–1882.

Berger, S., Cochrane, D., Simons, K., Savov, I.P., Ryan, J.G., Peterson, V.L., 2001. Insights from rare earth elements into the genesis of the Buck Creek Complex, Clay County, NC. Southeastern Geology, 40, 201–212.

Bodinier, J.L., Dupuy, C., Dostal, J., 1988. Geochemistry and petrogenesis of eastern Pyrenean peridotites. Geochim. Cosmochim. Acta 52, 2893–2907.

Bowring, S.A., Erwine, D.H., 1998. A new look at evolutionary rates in deep time: uniting paleontology and high-precision geochronology. GSA Today 8 (9), 1–6.

Bowring, S.A., Grotzinger, J.P., Isachsen, C.E., Knoll, A.N., Pelechaty, S.M., Kolosov, P., 1993. Calibrating rates of Early Cambrian evolution. Science 261, 1293–1298.

BVSP Basaltic Volcanism Study Project, 1981. Pergamon Press, New York, pp. 132–150.

Compston, W., Williams, I.S., Kirchvink, J.L., Zichao, Z., Guogan, M.A., 1992. Zircon U–Pb ages for the Early Cambrian time scale. J. Geol. Soc. Lond. 149, 171–184.

Dabbah, M.E., Rogers, J.J., 1983. Depositional environments and tectonic significance of the Wajid Sandstone of southern Saudi Arabia. J. Afr. Earth Sci. 1 (1), 47–57.

Frey, F.A., Suen, C.J., Stockman, H.W., 1985. The Ronda high temperature peridotite: geochemistry and petrogenesis. Geochim. Cosmochim. Acta 49, 2469–2491.

Fryer, P., 1995. Geology of the Mariana Trough. In: Taylor, B. (Ed.), Backarc Basins: Tectonics and Magmatism. Plenum press, New York, pp. 237–274.

Goncouglu, M.C., 1997. Distribution of Lower Paleozoic rocks in the Western Black Sea Region, Turkey, Early Paleozoic evolution in NW Gondwana. In: Proceedings IGCP Project 351, Ankara, pp. 13–23.

Hawkins, J.W., 1995. The geology of Lau Basin. In: Taylor, B. (Ed.), Backarc Basins: Tectonics and Magmatism. Plenum Press, New York, pp. 63–130.

Haydoutov, I., 1991. Origin and evolution of the Precambrian Bakan-Carpathian ophiolite segment. Bulg. Acad. Sci. Sofia, 179 (in Bulgarian with English summary).

Haydoutov, I., 1989. Precambrian ophiolites Cambrian island arc and Variscan suture in South Carpathian-Balkan region. Geology 17, 905–908.

Haydoutov, I., Yanev, S., 1997. The Protomoesian microcontinent of the Balkan Peninsula — a peri Gondvanian piece. Tectonophysics 272, 303–313.

Herbert, R., Laurent, R., 1990. Mineral chemistry of the plutonic section of the Troodos ophiolite: new constrains for the genesis of arc-related ophiolites. In: Malpas, J., Moores, E.M., Panayiotou, A., Xenophontos, C. (Eds.), Ophiolites: Oceanic Crustal Analogues. Geol. Surv. Cyprus, Nicosia, Cyprus, pp. 149–163.

Hochstaedter, A.G., Gill, J.B., Kusakabe, M., Newman, S., Pringle, M., Taylor, B., Fryer, P., 1990. Volcanism in the Sumisu Rift 1: Major element, volatile, and stable isotope geochemistry. Earth Planet Sci. Lett. 100, 179–194.

Kalenic, M., 1986. First find of lower Cambrian in E Serbia-S. Carpathian mountains. Rev. Bulg. Geol. Soc. 58, 2.

Kalvacheva, R., 1986. Acritarch stratigraphy of the Ordovician system in Bulgaria. Abstract, Final field meeting, IGCP Project 5, Sardinia, Italy, pp. 38–43.

Kepezhinskas, P., Sorokina, N., Mamontova, S., Savichev, A., 1995. Rare Earth and Large Lithophile (Sr and Ba) element geochemistry of diabase dikes, hole 504 B, Costa Rica Rift, Leg 140, In: Proceedings of the ODP Science Results, 137/140, pp. 107–115.

Kolcheva, K., Jordanov, B., 1984. Ultramafics and rodingite-gabbro fragments of culmulative ophiolite in the region of Kopilovzi. W. Balkan — Abstracts, Conference Bulg. Geol. Soc. Mihailovgrad, p. 15.

Kröner, A., 1984. Late Precambrian plate tectonics and orogeny: a need to redefine the term Pan-African. In: Klerkx, J., Mishot, J. (Eds.). Afr. Geol.. Tervuren, Belgium, pp. 23–28.

Kröner, A., Reischman, T., Todt, W., Zimmer, M., Stern, R., Hussein, I., Maksour, M., Eyal, Y., Sassi, F., 1989. Timing, mechanism and geochemical patterns of arc accretion in Arabian–Nubian Shield and its extensions into Israel and Somalia. Int. Geol. Congress, 28, Washington, DC, Ab., p. 230.

Langmuir, C.H., Bender, J.F., Batiza, R., 1986. Petrologic and tectonic segmentation of the East Pacific Rise. Nature 322, 422–429.

Melson, W.G., Vallier, T.L., Wright T.L., Byerly, G., Nelen, J., 1976. Chemical diversity of abyssal volcanic glass erupted along Pacific, Atlantic, and Indian Ocean sea-floor. In: The Geophysics of the Pacific Ocean basin and its margin, AGU monograph, Washington, DC, pp. 351–367.

Murphy, J., Nance, R., 1995. Supercontinent model for the contrasting character of Late Proterozoic orogenic belt. Geology 19 (5), 469–472.

Nakamura, N., 1974. Determination of REE, Ba, Fe, Mg, Na and K in carbonaceous and ordinary chondrites. Geochim. Cosmochim. Acta 38, 757–775.

Nicolas, A., 1989. Structures of ophiolites and dynamics of oceanic lithosphere. Petrol. Struct. Geol., vol. 4. Kluwer Academic Publishers, Amsterdam, pp. 187–200.

Odin, G.S., Gale, N.H., Aurvay, B., Bielski, M., Dore, F., Lancelot, J.R., Pasteels, P., 1983. Numerical dating of Precambrian–Cambrian boundary. Nature 301, 21–23.

Pallister, J.S., Stacey, J.S., Fischer, L.B., Premo, W.R., 1988. Precambrian ophiolites of Arabia: Geologic settings, U–Pb geochronology, Pb isotope characteristics, and implications for continental accretion. Precambr. Res. 38, 1–54.

Pearce, J.A., 1982. Traces elements characteristics of lavas from destructive plate margins. In: Thorpe, R.S. (Ed.). Andesites. Wiley, New York, pp. 525–548.

Quadt, A.V., Peycheva, I., Haydoutov, I., 1998. U–Zr dating of Tcerni Vrah metagabbro, West Balkan, Bulgaria. Comput. Rend. Acad. Bulg. Sci. 51 (1–2), 86–89.

Rogers, J.J., Unrug, R., Sultan, M., 1995. Tectonic assembly of Gondwana, . J. Geodyn. 19 (1), 1–34.

Ryan, J.G., 1989. The systematics of Lithium, Berillium and Boron in young volcanic rocks, PhD dissertation, Columbia University, pp. 291–293.

Ryan, J.G., Langmuir, C.H., 1993. The systematics of of boron abundances in young volcanic rocks. Geochim. Cosmochim. Acta 57, 1489–1498.

Savov, I.P., 1999. Petrology and Geochemistry of the Precambrian Balkan-Carpathian Ophiolite, Bulgaria and Serbia. MS thesis. University of South Florida, p. 106.

Scotese, C.R., 1997. Continental Drift, 7th edition, PALEOMAP Project, Arlington, Texas, 79 pp.

Scott, D.J., St-Onge, M.R., Lucas, S.B., Helmstaedt, H., 1991. Geology and chemistry of the early Proterozoic Purtuniq ophiolite. In: Peters, T.J., Nicolas, A., Coleman, R.G. (Eds.), Ophiolite Genesis and Evolution of the Oceanic Lithosphere. Kluwer Academic Publishers, Dordrecht, pp. 818–844.

Serri, G., 1981. The petrochemistry of ophiolite gabbroic complexes: a key for the classification of ophiolites into low-Ti and high-Ti. Earth Planet. Sci. Lett. 52, 203–212.

Shervais, J.W., 1982. Ti vesrsus V plots and the petrogenesis of modern and ophioitic Lavas. Earth Planet Sci. Lett. 59, 101–118.

Staudigel, H., Hart, S.R., 1983. Alteration of basaltic glass: mechanisms and significance for the oceanic seawater budget. Geochim. Cosmochim. Acta. 47, 337.

Stern, R.J., Hedge, E.C., 1985. Geochronologic and isotopic constraints on Late Precambrian crustal evolution in the Eastern Dessert of Egypt. Am. J. Sci. 285, 97–127.

Stern, R.J., Nielsen, K.C., Best, E., Sultan, M., Arvidson, R.E., Kroner, A., 1990. Orientation of late precambrian sutures in the Arabian–Nubian Shield. Geology 18, 1103–1106.

Stoeser, D., Camp, V., 1985. Pan-African microplate accretion of Arabian shield. Geol. Soc. Am. Bull. 96, 817–826.

Stolper, E., Newman, S., 1994. The role of water in the petrogenesis of Mariana Trough magmas. Earth. Planet. Sci. Lett. 121, 293–325.

Sultan, M., Becker, R., Arvidson, R.E., Shore, P., Stern, R.J., El Alfy, Z., Attia, R.I., 1993. New Constraints on Red Sea rifting from correlations of Arabian and Nubian Neoproterozoic outcrops. Tectonics 12 (6), 1303–1319.

Tenthorey, E.A., Ryan, J.G., Snow, A.E., 1996. Petrogenesis of sapphirine-bearing metatroctolites from the Buck Creek ultramafic body, southern Appalachians. J. Metamorphic Geol. 14, 103–114.

Terzic, M., 1981. Geosynclinal igneous activity in the Caledonian–Variscan cycle of Eastern Serbia. In: Petrovic, K. (Ed.), Geology

of Serbia, 3–1, Magmatism. University of Belgrade, Belgrade, pp. 33–47 (in Serbo-Croatian).

Unrug, R., 1993. The Gondwana supercontinent: Middle Proterozoic crustal fragments, Late Proterozoic assembly and unresolved problems. In: R.H. Finlay, R. Unrug, M.R. Banks, J.J. Veevers, (Eds), Proceedings of the Eighth Gondwana Symposium. A.A. Balkema, Rotterdam, pp. 3–8.

Ustaömer, P.A., Kipman, E., 1997. Remnant of Pre-Early Ordovician Cadomian active margin in West Pontides, N. Turkey. Terra Nova 9, 382.